Published in final edited form as:

Biol Psychiatry Cogn Neurosci Neuroimaging. 2019 June ; 4(6): 533–542. doi:10.1016/j.bpsc.2018.12.002.

Awake mouse imaging: from 2-photon microscopy to BOLD fMRI

Michèle Desjardins[#1,#], **Kıvılcım Kılıç**[#2,†], **Martin Thunemann**[1], **Celine Mateo**[3], **Dominic Holland**[2], **Christopher G.L. Ferri**[2], **Jonathan A. Cremonesi**[4], **Baoqiang Li**[5], **Qun Cheng**[2], **Kimberly L. Weldy**[2], **Payam A. Saisan**[2], **David Kleinfeld**[3,6,7], **Takaki Komiyama**[2,6], **Thomas T. Liu**[1], **Robert Bussell**[1], **Eric C. Wong**[1], **Miriam Scadeng**[1], **Andrew K. Dunn**[8], **David A. Boas**[9], **Sava Sakadžić**[5], **Joseph B. Mandeville**[5], **Richard B. Buxton**[1], **Anders M. Dale**[1,2], and **Anna Devor**[1,2,5]

[1]Department of Radiology, University of California San Diego, La Jolla, CA 92093, USA

[2]Department of Neurosciences, University of California San Diego, La Jolla, CA 92093, USA

[3]Department of Physics, University of California San Diego, La Jolla, CA 92093, USA

[4]Biology Undergraduate Program, University of California San Diego, La Jolla, CA 92093, USA

[5]Martinos Center for Biomedical Imaging, MGH, Harvard Medical School, Charlestown, MA 02129, USA

[6]Section of Neurobiology, University of California San Diego, La Jolla, CA 92093, USA

[7]Department of Electrical and Computer Engineering, University of California San Diego, La Jolla, CA 92093, USA

[8]Department of Biomedical Engineering, University of Texas at Austin, Austin, TX 78712, USA

[9]Department of Biomedical Engineering, Boston University, Boston, MA 02215, USA

[#] These authors contributed equally to this work.

Abstract

Background.—Functional Magnetic Resonance Imaging (fMRI) in awake behaving mice is well positioned to bridge the detailed cellular-level view of brain activity, which has become available due to recent advances in microscopic optical imaging and genetics, to the macroscopic scale of human noninvasive observables. However, while microscopic (e.g., 2-photon imaging) studies in behaving mice have become a reality in many laboratories, awake mouse fMRI remains a

Corresponding author: Michèle Desjardins, 2705, boulevard Laurier, Québec (Québec), Canada G1V 4G2, Tel: (418) 525-4444 #47531 or (418) 656-2131 #402783, michele.desjardins@phy.ulaval.ca.

[#]Present Address: Département de physique, de génie physique et d'optique, Université Laval and Centre de recherche du CHU de Québec – Université Laval, axe Oncologie, Québec, QC G1V 0A6, Canada;

[†]Present Address: Department of Biomedical Engineering, Boston University, Boston, MA 02215, USA

Financial Disclosure

The authors report no biomedical financial interests or potential conflicts of interest.

challenge. Furthermore, due to variability in behavior between animals, performing all types of measurements within the same subject is highly desirable and can lead to higher scientific rigor.

Methods.—Here, we demonstrate Blood Oxygenation Level Dependent (BOLD) fMRI in awake mice implanted with chronic "cranial windows" that allow optical access for microscopic imaging modalities and optogenetic (OG) stimulation. We start with 2-photon imaging of single-vessel diameter changes (N=1). Next, we implement intrinsic optical imaging of blood oxygenation and flow combined with laser speckle imaging of blood flow obtaining a "mesoscopic" picture of the hemodynamic response (N=16). Then, we obtain corresponding BOLD fMRI data (N=5). All measurements can be performed in the same mice in response to identical sensory and OG stimuli.

Results.—The cranial window does not deteriorate the quality of fMRI and allows alternating between imaging modalities in each subject.

Conclusions.—This report provides a proof of feasibility for multiscale imaging approaches in awake mice. In the future, this protocol can be extended to include complex cognitive behaviors translatable to humans, such as sensory discrimination or attention.

Keywords

2-photon microscopy; fMRI; Blood Oxygen Level Dependent (BOLD) signal; intrinsic optical signals; cerebral blood flow; optogenetic

Introduction

Noninvasive imaging technologies such as functional Magnetic Resonance Imaging (fMRI), Positron Emission Tomography (PET) and Electro/Magnetoencephalography (EEG/MEG) are widely used to investigate the function of the human brain. However, interpretation of these macroscopic signals in terms of the underlying microscopic physiology, such as electrical activity of single neurons and hemodynamic activity of single blood vessels, is still under investigation (1). Noninvasive imaging in experimental animals can play a critical role in physiological underpinning and data-driven modeling of human noninvasive signals, in particular when both micro- and macroscopic measurements are achieved in the same subject under analogous experimental conditions.

The idea is to utilize state-of-the-art microscopic measurement technologies in the mouse to precisely and quantitatively probe concrete microscopic physiological parameters underlying macroscopic cerebral blood flow, O_2 consumption, and electrophysiological EEG/MEG signals, while manipulating cell-type-specific neuronal activity (1). These measurements, which are only available in animals, provide the data needed for building computational bridges across spatial scales and imaging/recording modalities. For example, these microscopic measurements can be used to simulate the Blood Oxygenation Level Dependent (BOLD) fMRI signal "bottom-up" (2–5). The endpoint result can then be validated against the actual mouse fMRI data (2). These simulations also provide the microscopic "ground truth" for the development and calibration of "top-down" macroscopic analytical fMRI models applicable to humans (6).

Our previous studies relied on fMRI data from anesthetized rodents. However, anesthesia can differentially affect neuronal cell types – as well as blood flow and O_2 metabolism – altering neuronal network activity and neuro-vascular-metabolic coupling. To this end, the current report provides a protocol and a proof of feasibility for BOLD fMRI in awake mice implanted with chronic glass “cranial windows” that do not significantly deteriorate the quality of fMRI. These windows provide optical access for micro- and “mesoscopic” optical imaging modalities and neuronal stimulation with light (a.k.a. “optogenetics” (7)). Therefore, alternating between the imaging modalities for each subject is possible.

Mice have become the species of choice for detailed, microscopic *in vivo* imaging studies of the mammalian brain. This is in part due to recent advances in transgenic technology that allow genetically-targeted observation and manipulation of specific neuronal cell types. Novel genetically encoded probes of brain activity (e.g., genetically encoded calcium indicators, GECIs), as well as tools for optogenetic (OG) neuronal excitation and inhibition, have enabled new experimental paradigms where awake mice undergo repeated microscopic imaging, for the duration of weeks and months, while performing behavioral tasks (8). These chronic imaging studies are free from confounds of anesthesia and have a higher potential for human translation.

While optical imaging studies in awake and behaving mice have become routine, their fMRI counterpart remains a challenge. Prior studies have leveraged the power of noninvasive fMRI in intact conscious rodents to map the brain response to drug administration (9) and sensory stimuli, including tactile (10) and nociceptive somatic inputs (11) as well as odorants (12) and conditioned visual stimuli (13). Following the first demonstration of feasibility for combining fMRI with optogenetics by Lee and colleagues (14), the repertoire of stimuli applicable to awake rodent fMRI has been extended to include OG excitation or inhibition (15–19). In these studies, the OG light stimulus was delivered via an optical fiber implanted into the brain. In the present study, we employ a chronic cranial window that allows OG stimulation as well as singe- and multiphoton optical imaging of the cortical area within the window, enabling multiscale/multimodal imaging for each experimental subject. First, we describe installation and stability of our MRI-compatible headpost assembly including the cranial window. Then, we provide example data using optical imaging and fMRI in response to OG and sensory stimuli. In the present study, we used a simple air puff sensory stimulus. In the future, this protocol can be extended to include more complex cognitive behaviors translatable to humans, such as sensory discrimination or attention.

Methods

Some of the procedures were similar to those described in our previous study (20). For brevity, only novel aspects are described here. Detailed methods can be found in the Supplementary Methods.

Animal procedures

The surgical procedure was modified from that previously described by the Anderman lab (21) (see Supplementary Methods for details). The left barrel cortex was exposed over a 3-mm diameter circle area with the center coordinates of A-P 2 mm and L-R 3 mm (relative to

Bregma) and sealed with the glass window implant (Fig. 1A). A plastic headpost, used for immobilization of the head during imaging, was glued to the bone contralateral to the glass implant (Fig. 1B). To standardize the position of the imaging window across subjects, the headpost was lowered onto the bone while mounted onto a stereotactic manipulator ensuring a fixed angle and orientation.

Imaging

Following behavioral training, the animals were imaged using two-photon microscopy for single-vessel diameter measurements, spectral and laser speckle (LS) contrast imaging to measure blood oxygenation and flow, and BOLD fMRI. The BOLD fMRI methods are presented below; other methods can be found in the Supplementary Methods.

BOLD fMRI

MR images were acquired on a 7T/11 cm horizontal bore scanner (BioSpec 70/20 USR, Bruker) 7T scanner equipped with a BGA 12S2 gradient set with 440 mT/m gradient strength and 3440 T/m/s slew rate. A custom-made 2×3 cm diameter surface RF coil was used to transmit and receive the radiofrequency signal. BOLD fMRI data were acquired using a single-shot gradient-echo (GE) echo planar imaging (EPI) pulse sequence with the following parameters: TE/TR/FA = 11-20 ms / 1 s / 45° matrix = 100 (Read, L/R) × 50 (PE, S/I) over a 2×1 cm FOV, slice thickness = 1 mm, 5 adjacent coronal slices in interleaved order. High-resolution Rapid Acquisition with Relaxation Enhancement (TurboRARE) structural images were obtained of the same slices to identify brain structures and the location of the optical window (Supplementary Fig. S5). TurboRARE images had the same slice thickness as EPI images but higher in-plane resolution (256×128 for TurboRARE vs. 100×50 for EPI).

Mice were briefly (< 60s) anesthetized during the head fixation in a custom-made MRI-compatible mouse cradle (Supplementary Fig. S1C) and insertion of ear plugs (cut from commercial human-size silicon ear plugs). Once in the bore, coil stability was insured by inflating three pneumatic air chambers of the cradle to absorb vibrations. After manual coil matching and tuning, images were acquired in the following order: an anatomical localizer (TurboRARE), GE-EPI functional scans, spin-echo (SE) in forward and reverse directions for distortion correction (see below).

Motion correction was implemented by aligning each EPI image in a time series to the first one using in-house written rigid body registration software based on *imregister* Matlab function. Correction of image distortion due to B_0 field inhomogeneity induced by magnetic susceptibility variations was implemented using our previously published method that involves acquisition of two SE images with opposite phase encoding directions (22). EPI images were spatially smoothed with a 3-pixel FWHM Gaussian kernel. Ratio images were defined relative to a pre-stimulus baseline (2 s for event-related design, 5 s for blocked design) and averaged over stimulus trials. Realigned, smoothed images were entered into a general linear model (GLM) using SPM12 (Wellcome Trust Centre for Neuroimaging) and a canonical HRF with time derivatives. Using a finite impulse response model (FIR) yielded very similar results (not shown). A T-statistic contrast was used to identify voxels where the

signal significantly differed from baseline, i.e. activated voxels. The statistical map was thresholded at p = 0.001 uncorrected to define an ROI for time-course extraction.

Stimulus paradigm

For sensory stimulation, each trial consisted of a 2-s train of air puffs at 3 Hz delivered to the lower bottom part of the contralateral whisker pad to avoiding an eye blink; we used 10 trials per run with 20-s inter-stimulus interval, ISI. For the blocked stimulus, the puffs were delivered at 5 Hz for 20 s. During OG stimulation, each trial consisted of a train of 5-ms blue light pulses delivered at 100 Hz during 100 ms (equivalent to a single 100-ms pulse at 50% duty-cycle); we used 10 trials per run with 20-s ISI. For the blocked stimulus, the 100-ms trains were repeated at 1 Hz for 20 s with 8 trials per run. In fMRI and IOI/SC imaging, the OG light was delivered to the surface of the window by means of an optical fiber placed ~0.5 mm above the glass window creating a ~1 mm circular illumination spot. In 2-photon experiments, the OG light was delivered through the objective (20). Laser power was 6-8 mW under the objective (for 2-photon imaging) or at the fiber tip (for OIS/LS imaging). In the control experiments in wild type mice, laser power at the tip of the fiber was 12 mW.

Results

The goal for this study was to establish a protocol for chronic imaging of awake behaving mice using different measurement modalities, including 2-photon imaging and fMRI, in each subject. Our criteria for success were as follows: (1) sufficient optical clarity of the window to allow 2-photon imaging throughout the cortical depth as well as single-photon imaging; (2) minimal loss of the BOLD fMRI signal due to unwanted susceptibility artifacts; (3) sufficient mechanical stability of the MRI-compatible headpost assembly to allow state-of-the-art 2-photon imaging under analogous head fixation to that used in fMRI experiments; (4) stability over time for longitudinal imaging for the duration of weeks and months; (5) compatibility with behavioral experiments. Below, we describe our design and illustrate the imaging capabilities.

MRI-compatible headpost assembly

We used glass window implants previously described by Mark Anderman's lab (21). The implant was prepared ahead of time and consisted of three 3-mm round coverslips and a single 5-mm coverslip, all made of borosilicate glass (#1 thickness, Warner Instruments 64-0720 (CS-3R) and 64-0700 (CS-5R)) and glued together using optical adhesive (NOA61, Norland) that was cured with UV light (Spot Cure-B6, Kinetic Instruments) (Fig. 1A). The headpost, needed for immobilization of the mouse head during imaging, was custom machined from polyether ether ketone (PEEK), an MRI-compatible hard plastic material (Fig. 1B). Premade glass window implants and PEEK headposts were kept in 70% ethanol until implantation.

Borosilicate glass differs from the brain tissue (mostly composed of H_2O) in its magnetic susceptibility index (23). For 2D pulse sequences using relatively thick slices (in our case, 1 mm), this mismatch can lead to a susceptibility signal loss due to within-voxel, through-plane variation of the B_0 field. Therefore, we standardized the position of the imaging

window to ensure alignment of the glass/brain interface with the B_0 vector of the MRI scanner. To this end, the window and the headpost were fixed to the skull in a predetermined orientation such that, when the mouse head was immobilized in the MRI "cradle", the normal to the window plane would be orthogonal to B_0 (see Methods). In this way, susceptibility artifacts due to the window were limited to the perimeter of the implant.

In agreement with previous studies that utilized this type of cranial implants for 2-photon imaging (21), the window remained clear and transparent for the duration of weeks and months (Fig. 1C) allowing imaging throughout the cortical depth and down to the white matter (Fig. 1D). The quality of BOLD fMRI images depended to a large extent on the quality of the surgical preparation. Even after weeks of healing, residues of dry blood on the skull around the implant created signal loss and image distortion due to B_0 field inhomogeneity induced by magnetic susceptibility variations. Image distortion was corrected using our previously published method that involves acquisition of spin-echo (SE) echo-planar imaging (EPI) scans with opposite phase encoding polarities (22). Reversing the phase encoding direction resulted in opposite spatial distortion patterns. These data were then used to recover the correct image geometry of the target gradient-echo (GE) EPI scan (Fig. 1E and Supplementary Fig. S1A-B).

In all cases, BOLD fMRI images experienced some degree of signal loss at the edge of the borosilicate glass implant (Fig. 1E, red arrows). This artifact, however, was well localized to the perimeter of the window and did not significantly affect the quality of the BOLD signal immediately under the implant.

Compatibility with optical imaging across scales

Cranial glass windows allow optical imaging across scales that can be very informative for physiological underpinning of fMRI signals (20, 24, 25), in particular when the fMRI study is conducted in the same animal subject. On the microscopic scale, neuronal, glial, vascular and metabolic activity can be measured with sub-micron resolution using 2-photon imaging. Figure 2A-C illustrates an example of time-resolved imaging of single-vessel dilation, which is a key parameter in detailed models of fMRI signals (2, 6). These data were obtained by an intravascular injection of a fluorescent contrast agent (FITC or Alexa 680 conjugated to dextran, see Supplementary Methods) and tracking the vessel diameter as a function of time. In this example, we used a VGAT-ChR2(H134R)-EYFP mouse where all inhibitory interneurons expressed the OG actuator Channelrhodopsin-2 (ChR2) (26). The OG stimulus consisted of a single 100-ms pulse of blue (473 nm) light delivered through the objective (20). In addition, we used a sensory stimulus, which consisted of three air puffs delivered at 3 Hz to the whisker pad contralateral to the imaging window. If desired, 2-photon imaging can be used to extract other parameters including measures of neuroglial activity (24, 27–29), intravascular or tissue oxygenation (30–34), O_2 consumption (35), and glucose metabolism (36). Figure 2D-E and Supplementary Figure S2A show the corresponding mesoscopic changes in blood oxygenation and flow obtained in the same subject under the same stimulus conditions using single-photon CCD-based imaging. In this example, we used simultaneous hemoglobin-based optical intrinsic signals (OIS) imaging and LS contrast imaging (37–39) to obtain changes in oxyhemoglobin (HbO), deoxyhemoglobin (HbR) and

blood flow in response to OG and sensory stimulation. The OG stimulus was delivered via an optical fiber positioned ~0.5 mm above the window at an angle of ~60 degrees to avoid reflection from the glass surface (Fig. 2D**)** using the same stimulus parameters as for 2-photon imaging shown in Figure 2C. Presenting the same OG stimulus in wild type animals did not cause significant HbO/HbR changes (Supplementary Fig. S2B), arguing against potential effects of heat generated by the 473-nm laser within our range of laser power (40, 41). The sensory stimulus was the same as for 2-photon measurements (Fig. 2C). For 2-photon imaging, we rejected stimulus trials with large motion artifacts that could be identified by analysis of the surveillance video (see Methods) and/or unrealistically large signal changes. Sensory stimuli generated motion more often compared to OG stimuli: ~15-20% of trials were rejected for sensory stimuli and ~5-10% - for OG stimuli. OIS imaging is more robust against motion artifacts, thus no trials were rejected. Some studies used sedation to mitigate motion artifacts (27). In our hands, however, sedation with 1-2 mg/kg chlorprothixene (Sigma-Aldrich) notably slowed down the hemodynamic response kinetics (Supplementary Fig. S2C). Thus, sedation is not recommended as a means of providing image stability in quantitative hemodynamic and neurovascular coupling studies.

BOLD fMRI in mice with chronic cranial windows

Mesoscopic OIS and LS contrast measures can serve as a proxy for the BOLD fMRI signal (42–45). However, the measurement theory for each of these measurement modalities is unique, relying on different assumptions across different imaging modalities (46). Therefore, direct acquisition of the fMRI data is highly desirable to ensure consistency of the modeling/integration framework (1, 2). To this end, we performed BOLD fMRI in mice with chronic cranial windows in response to OG and sensory stimulation. OG stimulus was delivered via an optical fiber similar to that used in the OIS/LS experiments. The fiber was positioned in the middle of the RF coil ending ~0.5 mm above the glass window at an angle of ~70 degrees (see Methods and Supplementary Fig. S1C). Since we used a small surface RF coil to transmit and receive (see Methods), our sensitivity dropped with distance from the coil resulting in an inhomogeneous signal-to-noise ratio (SNR) within the image. Therefore, we thresholded EPI images at ~40% of the maximum intensity to limit our analysis to pixels with high SNR. Figure 3 illustrates BOLD fMRI responses to a 20-s train of 100-ms light pulses delivered at 1 Hz (Fig. 3A-C, analogous to a blocked design) and a single 100-ms light pulse (Fig. 3D-E, analogous to an event-related design) from a single fully awake Emx1-Cre/Ai32 subject where ChR2 was expressed in pyramidal cells (47, 48). BOLD ratio images (Fig. 3A, D) were calculated relative to the pre-stimulus baseline using a single slice cutting through the center of the evoked response. This presentation facilitates the comparison with OIS imaging if needed (25). The BOLD signal change in response to both stimulus conditions localized to the cortical tissue within the cranial window. The same data can also be viewed as p-value maps; statistically significant activation localized to the cortical area within the window was detected for the blocked design (Fig. 3C). Time-courses extracted from the active ROI, which was defined by thresholding of the p-value map, revealed a high degree of temporal signal fluctuation (Fig. 3B,E and Supplementary Fig. S3), most likely due to spontaneous neuronal activity (49, 50) as well as residual movement artifacts. On average, an increase in the BOLD signal was visible for both stimulus conditions (thick lines in Fig. 3B,E and Supplementary Fig. S3). Comparison of the BOLD

response time-course to that obtained by OIS/LS imaging revealed a consistent shape across the measurement modalities for the same stimulus condition (Supplementary Fig. S4).

Sensory stimulus in fMRI experiments consisted of air puffs delivered at 3-5 Hz to the whisker pad contralateral to the cranial window for a total duration of 20 s ("blocked" design) or 2 s ("event-related" design). Figure 4 shows an example BOLD response in a fully awake mouse. As for the OG stimulus, BOLD signal change in response to both stimulus conditions localized to the cortical region within the window (Fig. 4A,D), and an increase in the BOLD signal was visible for both stimulus conditions in trial-averaged time-courses (Fig. 4B,E). Statistically significant activation was detected for the blocked design (Fig. 4C). As with 2-photon imaging, we rejected stimulus trials with significant motion identified by analysis of the surveillance video (see Methods and Supplementary Movie 1). When significant motion occurred somewhere within a stimulus trial, we always rejected the entire trial. The proportion of rejected trials was similar to that in 2-photon imaging: ~15-20% and ~5-10% for sensory and OG stimuli, respectively.

In contrast to Figures 3 and 4 where the mouse was fully awake, Figure 5 shows fMRI data acquired under sedation with chlorprothixene. In this case, we observed a larger spread of OG-induced activity, including the contralateral hemisphere (Fig. 5A). The highest BOLD response, however, was well mapped to the cortical tissue under the window (Fig. 5B). Sedated animals had lower baseline signal fluctuations, probably explained by reduced neuronal activity and body movement (Fig. 5C-D and Supplementary Fig. S3). Thus, while not appropriate for quantitative hemodynamic studies (Supplementary Fig. S2C), BOLD fMRI in sedated mice may still be useful for troubleshooting the protocol and procedure. This is due to high SNR of the BOLD signal and limited motion artifacts in sedated animals. Also, no trials were rejected due to motion under sedation.

Discussion

In the present study, we have achieved BOLD fMRI in fully awake mice, chronically implanted with optical windows, in response to sensory and OG stimuli. Compared to our published data from rats anesthetized with α-chloralose (25), the BOLD signal induced by sensory stimulation in awake mice was ~3 times smaller when normalized by the corresponding averaged arteriolar dilation (awake mice in the present study: ~0.5% BOLD, ~7% dilation; anesthetized rats in Tian et al. (2010): ~2% BOLD, ~10% dilation). This difference can be caused by slower baseline blood flow under anesthesia leading to an increase in the fraction of O_2 extracted from blood by tissue. Hypothetically, if the baseline neuronal activity and cerebral metabolic rate of O_2 ($CMRO_2$) remain the same, slower flow would lead to a higher O_2 extraction fraction resulting in higher amount of HbR in the voxel and lower baseline level of the BOLD signal. Thus, we speculate that if α-chloralose anesthesia affects the baseline blood flow more that it affects neuronal activity and neurovascular coupling, the stimulus may produce a greater ΔBOLD signal between the baseline and stimulated conditions. An alternative explanation for the low BOLD response in response to sensory stimulation in the present study may be due to reduced attention of the animals to the stimulus during BOLD fMRI acquisition. Our animals were well trained and habituated to the noise of an echo planar imaging (EPI) pulse sequence used for BOLD

acquisition, head fixation and LED lighting, as well as to wearing protective ear plugs (see Methods). However, we cannot rule out that some environmental factors, e.g., a residual vibration transmitted through the air cushions, distracted the animals' attention to the air puff.

In conclusion, the present study provides a proof-of-principle demonstration for using chronic optical cranial windows in animal BOLD fMRI studies. These windows support multimodal optical imaging, from detailed 2-photon microscopy throughout the cortical depth and beyond to meso- and macroscopic optical imaging using all available optical contrasts mechanisms. We demonstrate that the presence of the window results in minimal losses of the BOLD fMRI signal while allowing OG stimulation by simply positioning an optical fiber next to the window. These windows are stable and support longitudinal imaging alternating between imaging modalities for each subject over weeks and months. In the future, sampling multiple physiological parameters in an awake behaving mouse across scales and measurement modalities, including BOLD fMRI, will be instrumental for bridging BOLD fMRI signals, induced by a complex behavior, to the underlying activity of neuronal circuits. The ability to perform longitudinal studies, while alternating between imaging modalities and manipulating neuronal activity with OG tools, can also facilitate neurophysiological underpinning of spontaneous ("resting state") hemodynamic fluctuations (49–52) as well as cortical MRI signals in response to clinically-relevant perturbations of brain activity (53).

Supplementary Material

Refer to Web version on PubMed Central for supplementary material.

Acknowledgments

We gratefully acknowledge support from the NIH (MH111359, NS057198, U01NS094232, and S10RR029050). M. Desjardins was supported by a postdoctoral scholarship from the Natural Sciences and Engineering Research Council of Canada. K. Kılıç was supported by a postdoctoral fellowship from the International Headache Society and TUBITAK. M. Thunemann was supported by a postdoctoral fellowship from the German Research Council (DFG TH 2031/1).

References

1. Uhlirova H, Kilic K, Tian P, Sakadzic S, Gagnon L, Thunemann M, et al. (2016): The roadmap for estimation of cell-type-specific neuronal activity from non-invasive measurements. Philos Trans R Soc Lond B Biol Sci. 371.
2. Gagnon L, Sakadzic S, Lesage F, Musacchia JJ, Lefebvre J, Fang Q, et al. (2015): Quantifying the microvascular origin of BOLD-fMRI from first principles with two-photon microscopy and an oxygen-sensitive nanoprobe. J Neurosci. 35:3663–3675. [PubMed: 25716864]
3. Gagnon L, Smith AF, Boas DA, Devor A, Secomb TW, Sakadzic S (2016): Modeling of Cerebral Oxygen Transport Based on In vivo Microscopic Imaging of Microvascular Network Structure, Blood Flow, and Oxygenation. Front Comput Neurosci. 10:82. [PubMed: 27630556]
4. Fang Q, Sakadzic S, Ruvinskaya L, Devor A, Dale AM, Boas DA (2008): Oxygen advection and diffusion in a three-dimensional vascular anatomical network. Opt Express. 16:17530–17541. [PubMed: 18958033]
5. Boas DA, Jones SR, Devor A, Huppert TJ, Dale AM (2008): A vascular anatomical network model of the spatio-temporal response to brain activation. Neuroimage. 40:1116–1129. [PubMed: 18289880]

6. Gagnon L, Sakadzic S, Lesage F, Pouliot P, Dale AM, Devor A, et al. (2016): Validation and optimization of hypercapnic-calibrated fMRI from oxygen-sensitive two-photon microscopy. Philos Trans R Soc Lond B Biol Sci. 371.
7. Deisseroth K (2015): Optogenetics: 10 years of microbial opsins in neuroscience. Nat Neurosci. 18:1213–1225. [PubMed: 26308982]
8. Makino H, Komiyama T (2015): Learning enhances the relative impact of top-down processing in the visual cortex. Nat Neurosci. 18:1116–1122. [PubMed: 26167904]
9. Ferris CF, Yee JR, Kenkel WM, Dumais KM, Moore K, Veenema AH, et al. (2015): Distinct BOLD Activation Profiles Following Central and Peripheral Oxytocin Administration in Awake Rats. Front Behav Neurosci. 9:245. [PubMed: 26441574]
10. Chang PC, Procissi D, Bao Q, Centeno MV, Baria A, Apkarian AV (2016): Novel method for functional brain imaging in awake minimally restrained rats. J Neurophysiol. 116:61–80. [PubMed: 27052584]
11. Yee JR, Kenkel W, Caccaviello JC, Gamber K, Simmons P, Nedelman M, et al. (2015): Identifying the integrated neural networks involved in capsaicin-induced pain using fMRI in awake TRPV1 knockout and wild-type rats. Front Syst Neurosci. 9:15. [PubMed: 25745388]
12. Ferris CF, Kulkarni P, Toddes S, Yee J, Kenkel W, Nedelman M (2014): Studies on the Q175 Knock-in Model of Huntington's Disease Using Functional Imaging in Awake Mice: Evidence of Olfactory Dysfunction. Front Neurol. 5:94. [PubMed: 25071696]
13. Harris AP, Lennen RJ, Marshall I, Jansen MA, Pernet CR, Brydges NM, et al. (2015): Imaging learned fear circuitry in awake mice using fMRI. Eur J Neurosci. 42:2125–2134. [PubMed: 25943794]
14. Lee JH, Durand R, Gradinaru V, Zhang F, Goshen I, Kim DS, et al. (2010): Global and local fMRI signals driven by neurons defined optogenetically by type and wiring. Nature. 465:788–792. [PubMed: 20473285]
15. Kolodziej A, Lippert M, Angenstein F, Neubert J, Pethe A, Grosser OS, et al. (2014): SPECT-imaging of activity-dependent changes in regional cerebral blood flow induced by electrical and optogenetic self-stimulation in mice. Neuroimage. 103:171–180. [PubMed: 25234116]
16. Liang Z, Watson GD, Alloway KD, Lee G, Neuberger T, Zhang N (2015): Mapping the functional network of medial prefrontal cortex by combining optogenetics and fMRI in awake rats. Neuroimage. 117:114–123. [PubMed: 26002727]
17. Aksenov DP, Li L, Miller MJ, Wyrwicz AM (2016): Blood oxygenation level dependent signal and neuronal adaptation to optogenetic and sensory stimulation in somatosensory cortex in awake animals. Eur J Neurosci. 44:2722–2729. [PubMed: 27564781]
18. Brocka M, Helbing C, Vincenz D, Scherf T, Montag D, Goldschmidt J, et al. (2018): Contributions of dopaminergic and non-dopaminergic neurons to VTA-stimulation induced neurovascular responses in brain reward circuits. Neuroimage. 177:88–97. [PubMed: 29723641]
19. Desai M, Kahn I, Knoblich U, Bernstein J, Atallah H, Yang A, et al. (2011): Mapping brain networks in awake mice using combined optical neural control and fMRI. J Neurophysiol. 105:1393–1405. [PubMed: 21160013]
20. Uhlirova H, Kilic K, Tian P, Thunemann M, Desjardins M, Saisan PA, et al. (2016): Cell type specificity of neurovascular coupling in cerebral cortex. Elife. 5.
21. Goldey GJ, Roumis DK, Glickfeld LL, Kerlin AM, Reid RC, Bonin V, et al. (2014): Removable cranial windows for long-term imaging in awake mice. Nat Protoc. 9:2515–2538. [PubMed: 25275789]
22. Holland D, Kuperman JM, Dale AM (2010): Efficient correction of inhomogeneous static magnetic field-induced distortion in Echo Planar Imaging. Neuroimage. 50:175–183. [PubMed: 19944768]
23. Wapler MC, Leupold J, Dragonu I, von Elverfeld D, Zaitsev M, Wallrabe U (2014): Magnetic properties of materials for MR engineering, micro-MR and beyond. J Magn Reson. 242:233–242. [PubMed: 24705364]
24. Nizar K, Uhlirova H, Tian P, Saisan PA, Cheng Q, Reznichenko L, et al. (2013): In vivo stimulus-induced vasodilation occurs without IP3 receptor activation and may precede astrocytic calcium increase. J Neurosci. 33:8411–8422. [PubMed: 23658179]

25. Tian P, Teng IC, May LD, Kurz R, Lu K, Scadeng M, et al. (2010): Cortical depth-specific microvascular dilation underlies laminar differences in blood oxygenation level-dependent functional MRI signal. Proc Natl Acad Sci U S A. 107:15246–15251. [PubMed: 20696904]
26. Zhao S, Ting JT, Atallah HE, Qiu L, Tan J, Gloss B, et al. (2011): Cell type-specific channelrhodopsin-2 transgenic mice for optogenetic dissection of neural circuitry function. Nat Methods. 8:745–752. [PubMed: 21985008]
27. Bonder DE, McCarthy KD (2014): Astrocytic Gq-GPCR-linked IP3R-dependent Ca2+ signaling does not mediate neurovascular coupling in mouse visual cortex in vivo. J Neurosci. 34:13139–13150. [PubMed: 25253859]
28. Monai H, Ohkura M, Tanaka M, Oe Y, Konno A, Hirai H, et al. (2016): Calcium imaging reveals glial involvement in transcranial direct current stimulation-induced plasticity in mouse brain. Nat Commun. 7:11100. [PubMed: 27000523]
29. Otsu Y, Couchman K, Lyons DG, Collot M, Agarwal A, Mallet JM, et al. (2015): Calcium dynamics in astrocyte processes during neurovascular coupling. Nat Neurosci. 18:210–218. [PubMed: 25531572]
30. Devor A, Sakadzic S, Saisan PA, Yaseen MA, Roussakis E, Srinivasan VJ, et al. (2011): "Overshoot" of O(2) is required to maintain baseline tissue oxygenation at locations distal to blood vessels. J Neurosci. 31:13676–13681. [PubMed: 21940458]
31. Sakadzic S, Roussakis E, Yaseen MA, Mandeville ET, Srinivasan VJ, Arai K, et al. (2010): Two-photon high-resolution measurement of partial pressure of oxygen in cerebral vasculature and tissue. Nat Methods. 7:755–759. [PubMed: 20693997]
32. Lecoq J, Parpaleix A, Roussakis E, Ducros M, Goulam Houssen Y, Vinogradov SA, et al. (2011): Simultaneous two-photon imaging of oxygen and blood flow in deep cerebral vessels. Nat Med. 17:893–898. [PubMed: 21642977]
33. Lyons DG, Parpaleix A, Roche M, Charpak S (2016): Mapping oxygen concentration in the awake mouse brain. Elife. 5.
34. Parpaleix A, Goulam Houssen Y, Charpak S (2013): Imaging local neuronal activity by monitoring PO(2) transients in capillaries. Nat Med. 19:241–246. [PubMed: 23314058]
35. Sakadzic S, Yaseen MA, Jaswal R, Roussakis E, Dale AM, Buxton RB, et al. (2016): Two-photon microscopy measurement of cerebral metabolic rate of oxygen using periarteriolar oxygen concentration gradients. Neurophotonics. 3:045005. [PubMed: 27774493]
36. Machler P, Wyss MT, Elsayed M, Stobart J, Gutierrez R, von Faber-Castell A, et al. (2016): In Vivo Evidence for a Lactate Gradient from Astrocytes to Neurons. Cell Metab. 23:94–102. [PubMed: 26698914]
37. Devor A, Sakadzic S, Yaseen MA, Roussakis E, Tian P, Slovin H, et al. (2013): Functional imaging of cerebral oxygenation with intrinsic optical contrast and phosphorescent probes In: Weber B, Helmchen F, editors. Optical imaging of cortical circuit dynamics. New York: Springer.
38. Dunn AK, Devor A, Bolay H, Andermann ML, Moskowitz MA, Dale AM, et al. (2003): Simultaneous imaging of total cerebral hemoglobin concentration, oxygenation, and blood flow during functional activation. Opt Lett. 28:28–30. [PubMed: 12656525]
39. Dunn AK, Devor A, Dale AM, Boas DA (2005): Spatial extent of oxygen metabolism and hemodynamic changes during functional activation of the rat somatosensory cortex. Neuroimage. 27:279–290. [PubMed: 15925522]
40. Christie IN, Wells JA, Southern P, Marina N, Kasparov S, Gourine AV, et al. (2013): fMRI response to blue light delivery in the naive brain: implications for combined optogenetic fMRI studies. Neuroimage. 66:634–641. [PubMed: 23128081]
41. Rungta RL, Osmanski BF, Boido D, Tanter M, Charpak S (2017): Light controls cerebral blood flow in naive animals. Nat Commun. 8:14191. [PubMed: 28139643]
42. Devor A, Dunn AK, Andermann ML, Ulbert I, Boas DA, Dale AM (2003): Coupling of total hemoglobin concentration, oxygenation, and neural activity in rat somatosensory cortex. Neuron. 39:353–359. [PubMed: 12873390]
43. Devor A, Ulbert I, Dunn AK, Narayanan SN, Jones SR, Andermann ML, et al. (2005): Coupling of the cortical hemodynamic response to cortical and thalamic neuronal activity. Proc Natl Acad Sci U S A. 102:3822–3827. [PubMed: 15734797]

44. Grinvald A, Sharon D, Omer D, Vanzetta I (2016): Imaging the Neocortex Functional Architecture Using Multiple Intrinsic Signals: Implications for Hemodynamic-Based Functional Imaging. Cold Spring Harb Protoc. 2016:pdb top089375.
45. Jones M, Berwick J, Johnston D, Mayhew J (2001): Concurrent optical imaging spectroscopy and laser-Doppler flowmetry: the relationship between blood flow, oxygenation, and volume in rodent barrel cortex. Neuroimage. 13:1002–1015. [PubMed: 11352606]
46. Devor A, Boas D, Einevoll GT, Buxton RB, Dale AM (2012): Neuronal Basis of Non-Invasive Functional Imaging: From Microscopic Neurovascular Dynamics to BOLD fMRI In: In-Young Choi RG, editor. Neural Metabolism In Vivo. New York: Springer.
47. Gorski JA, Talley T, Qiu M, Puelles L, Rubenstein JL, Jones KR (2002): Cortical excitatory neurons and glia, but not GABAergic neurons, are produced in the Emx1-expressing lineage. J Neurosci. 22:6309–6314. [PubMed: 12151506]
48. Madisen L, Mao T, Koch H, Zhuo JM, Berenyi A, Fujisawa S, et al. (2012): A toolbox of Cre-dependent optogenetic transgenic mice for light-induced activation and silencing. Nat Neurosci. 15:793–802. [PubMed: 22446880]
49. Ma Y, Shaik MA, Kozberg MG, Kim SH, Portes JP, Timerman D, et al. (2016): Resting-state hemodynamics are spatiotemporally coupled to synchronized and symmetric neural activity in excitatory neurons. Proc Natl Acad Sci U S A. 113:E8463–E8471. [PubMed: 27974609]
50. Mateo C, Knutsen PM, Tsai PS, Shih AY, Kleinfeld D (2017): Entrainment of Arteriole Vasomotor Fluctuations by Neural Activity Is a Basis of Blood-Oxygenation-Level-Dependent "Resting-State" Connectivity. Neuron. 96:936–948 e933. [PubMed: 29107517]
51. Murphy MC, Chan KC, Kim SG, Vazquez AL (2018): Macroscale variation in resting-state neuronal activity and connectivity assessed by simultaneous calcium imaging, hemodynamic imaging and electrophysiology. Neuroimage. 169:352–362. [PubMed: 29277650]
52. Schwalm M, Schmid F, Wachsmuth L, Backhaus H, Kronfeld A, Aedo Jury F, et al. (2017): Cortex-wide BOLD fMRI activity reflects locally-recorded slow oscillation-associated calcium waves. Elife. 6.
53. Albaugh DL, Salzwedel A, Van Den Berge N, Gao W, Stuber GD, Shih YY (2016): Functional Magnetic Resonance Imaging of Electrical and Optogenetic Deep Brain Stimulation at the Rat Nucleus Accumbens. Sci Rep. 6:31613. [PubMed: 27601003]

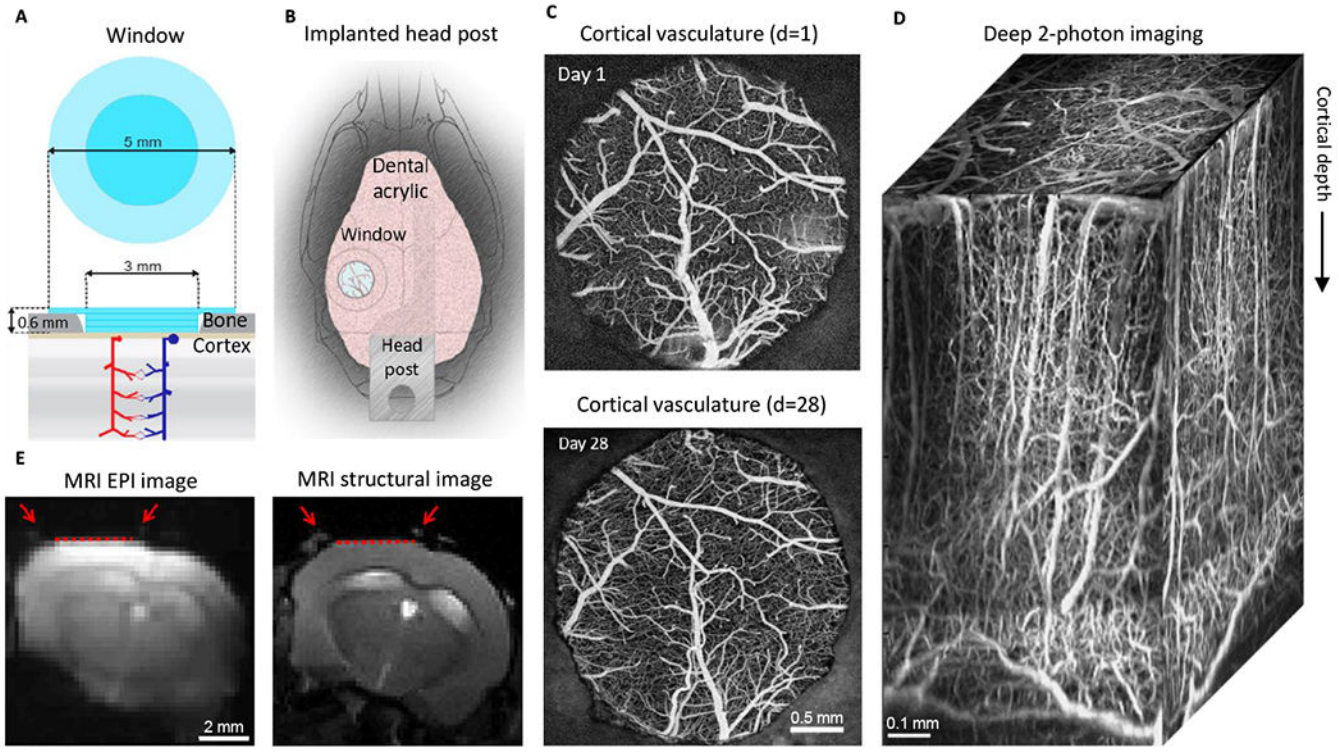

Figure 1. MRI-compatible headpost assembly and image quality across modalities

A. Schematics of the borosilicate glass window implant.

B. Schematic illustration of the window implant over the whisker representation within the primary somatosensory cortex (SI) and the headpost fixed to the skull overlaying the other (contralateral) hemisphere.

C. Images of the brain vasculature through the glass window implant obtained by 2-photon imaging of fluorescein isothiocyanate (FITC)-labeled dextran injected intravenously. The images illustrate preserved integrity of the vasculature between days 1 (top) and 28 (bottom) following surgical implantation.

D) Two-photon image stack obtained with Alexa 680 labeled dextran injected intravenously illustrating the capability of deep imaging.

E) Corrected GE EPI image (left) and a corresponding structural image (TurboRARE, right). Red arrows point to the peripheral edges of the implant, i.e., the glass/bone boundary. The red line indicates the bottom of the glass implant, i.e., the glass/brain boundary.

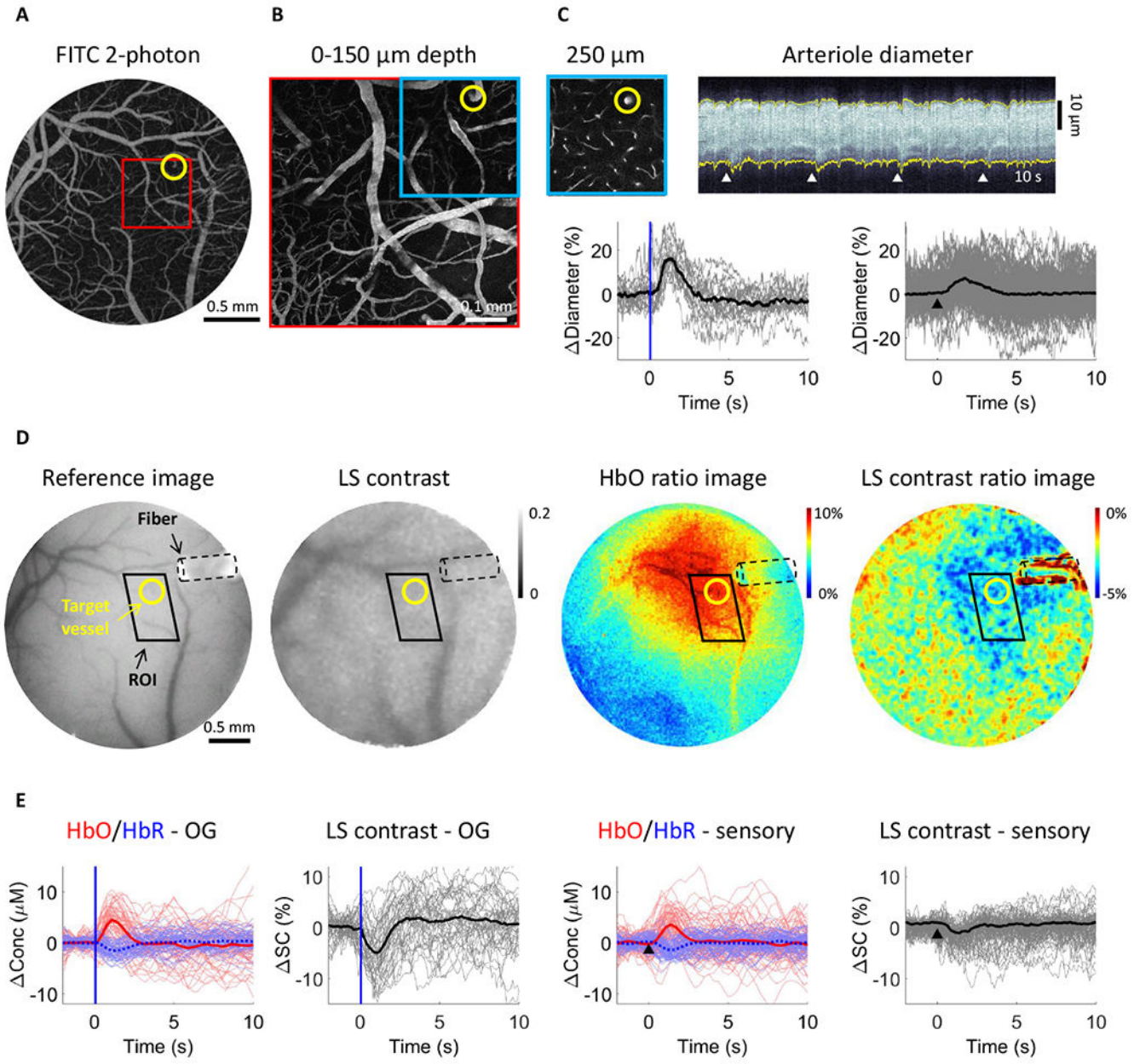

Figure 2. From 2-photon microscopy to mesoscopic OIS/LS imaging providing a proxy for the BOLD signal

A. Image of the surface vasculature calculated as a maximum intensity projection (MIP) of an image stack 0–300 µm in depth using a 4× objective. Individual images were acquired every 10 µm.

B. A zoomed-in view of the region within the red square in (A) acquired with a 20× objective.

C. Top left: A plane 250 µm below the surface corresponding to the region outlined in blue in (B). The yellow circle indicates a small diving arteriole. Top right: An example temporal diameter change profile acquired from the arteriole outlined by the yellow circle imaged 250 µm below the surface. The vessel diameter was captured by repeated line-scans across the

vessel. These line-scans form a space-time image when stacked sequentially, from left to right. White arrowheads indicate the onset of stimulus trials (air puffs to the whisker pad); four trials are shown. Bottom: Single-vessel dilation time-courses extracted from data such as that illustrated in (C). Time-courses for individual trials are overlaid for OG stimulus (left, n=19 trials) and sensory stimulus (right, n=160 trials); the thick lines show the average. The stimulus onset is indicated by the blue vertical line and a black arrowhead for the OG and sensory panels, respectively.

D. Concurrent OIS and LS contrast imaging in the same subject as in (A)-(C). Left: A CCD reflectance image of the surface vasculature. Middle: The corresponding LS contrast image. Right: Ratio images of HbO (extracted from the OIS data, see Methods) and LS contrast showing the region of activation following OG stimulation. The location of optical fiber is indicated on all images (black dotted line). The same arteriole as in (C) is outlined by yellow circles. The black parallelogram indicates the region of interest (ROI) used for extraction of time-courses in (E).

E. Time-courses of HbO and HbR (shown in red and blue, respectively) and LS contrast (shown in black) in response to OG and sensory stimulation. These time-courses were extracted from the polygonal ROI shown in (D).

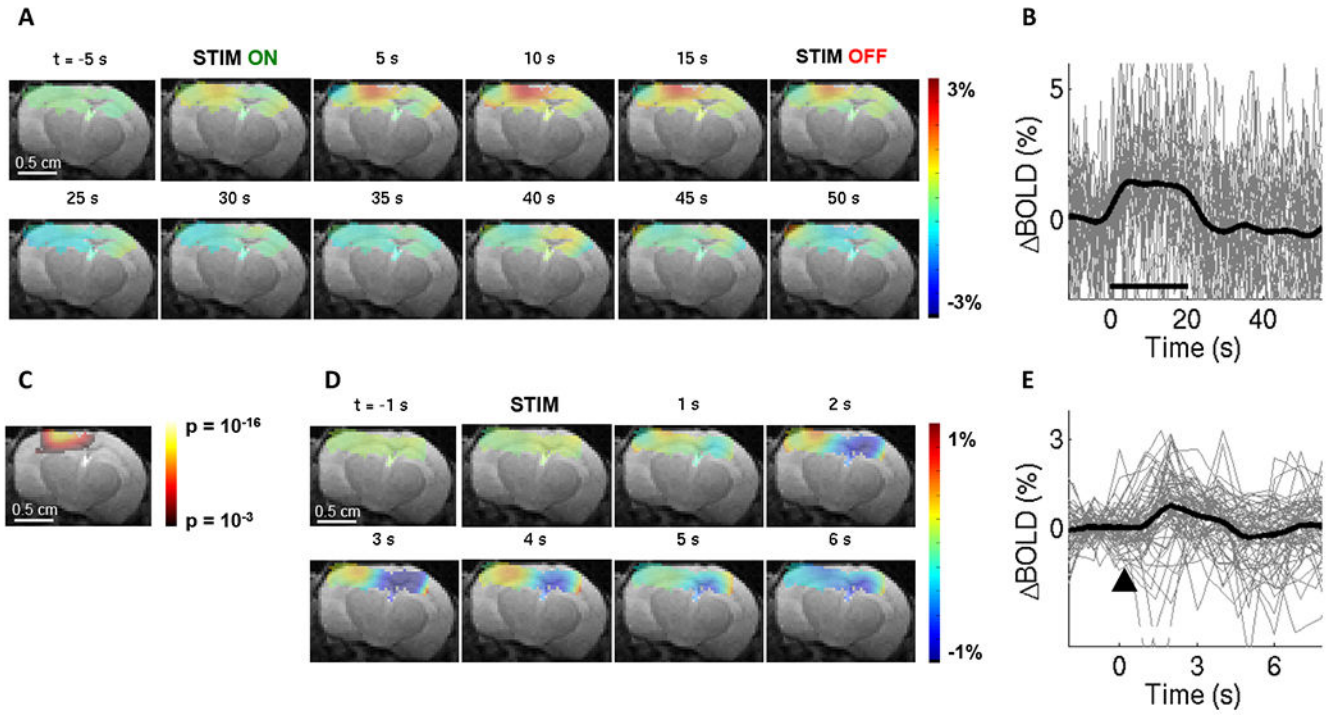

Figure 3. The BOLD signal in response to OG stimuli in a fully awake mouse

A. Spatiotemporal evolution of the BOLD signal change from a single slice cutting through the center of the evoked response, presented as trial-averaged ratio maps, in response to a 20-s train of 100-ms light pulses delivered at 1 Hz (“blocked” OG stimulus) in a single Emx1-Cre/Ai32 subject. EPI images were thresholded to reflect the sensitivity of the surface RF coil (for display purposes only). The ratio images are overlaid on the structural (TurboRARE) image of the same slice.

B. BOLD response time-courses extracted from the active ROI. 28 stimulus trials are superimposed. The average is overlaid in thick black. For the full range of the y-axis, see Supplementary Fig. S3.

C. Thresholded (p = 0.001 uncorrected) statistical p-map corresponding to the data shown in (A) assuming the standard hemodynamic response function (HRF) with temporal derivatives (see Mehods). This map was used to define the ROI for extraction of time-courses in (B) and (E).

D. As in (A) for single 100-ms light pulses (“event-related” OG stimulus) in the same subject.

E. BOLD response time-courses corresponding to (D). 69 stimulus trials are superimposed. The average is overlaid in thick black.

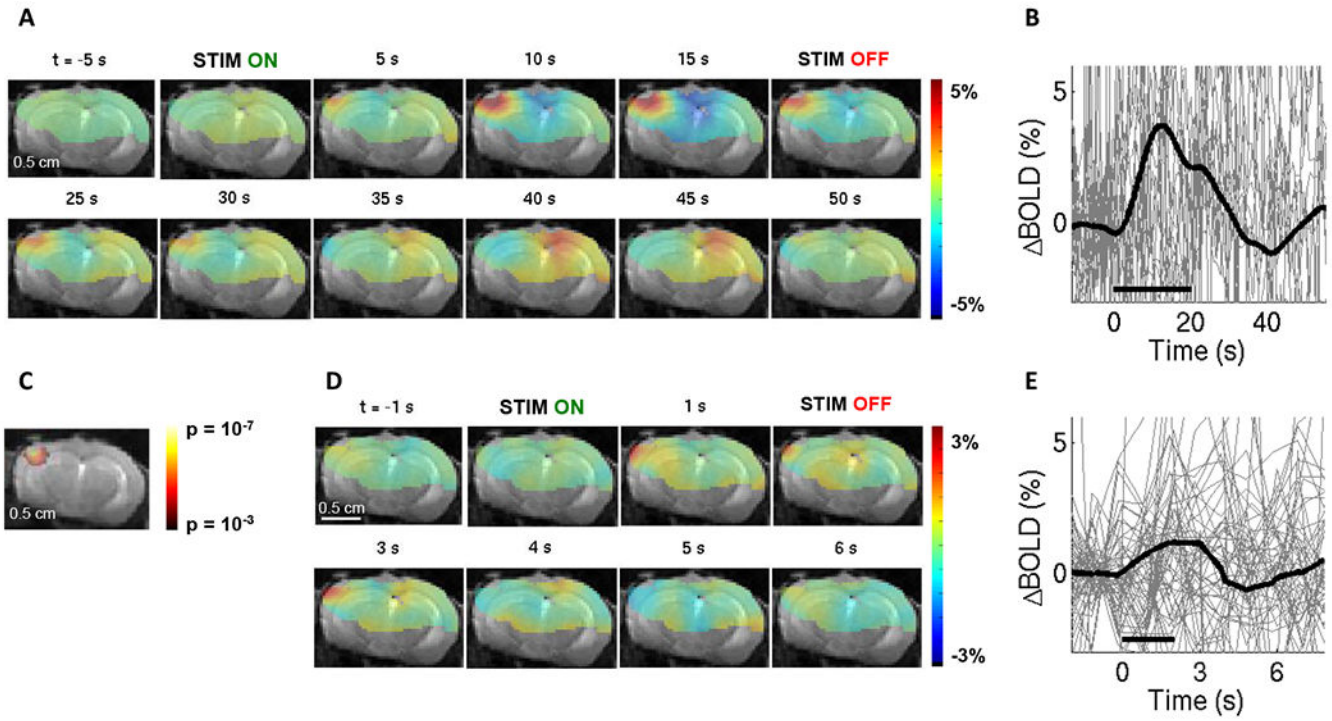

Figure 4. The BOLD signal in response to sensory stimuli in a fully awake mouse

Conventions are the same as in Fig. 3. (A)-(C) correspond to 20-s stimulus duration (n=21 trials). (D)-(E) correspond to 2-s stimulus duration (n=57 trials). For the full range of the y-axis for the BOLD signal time-courses, see Supplementary Fig. S3.

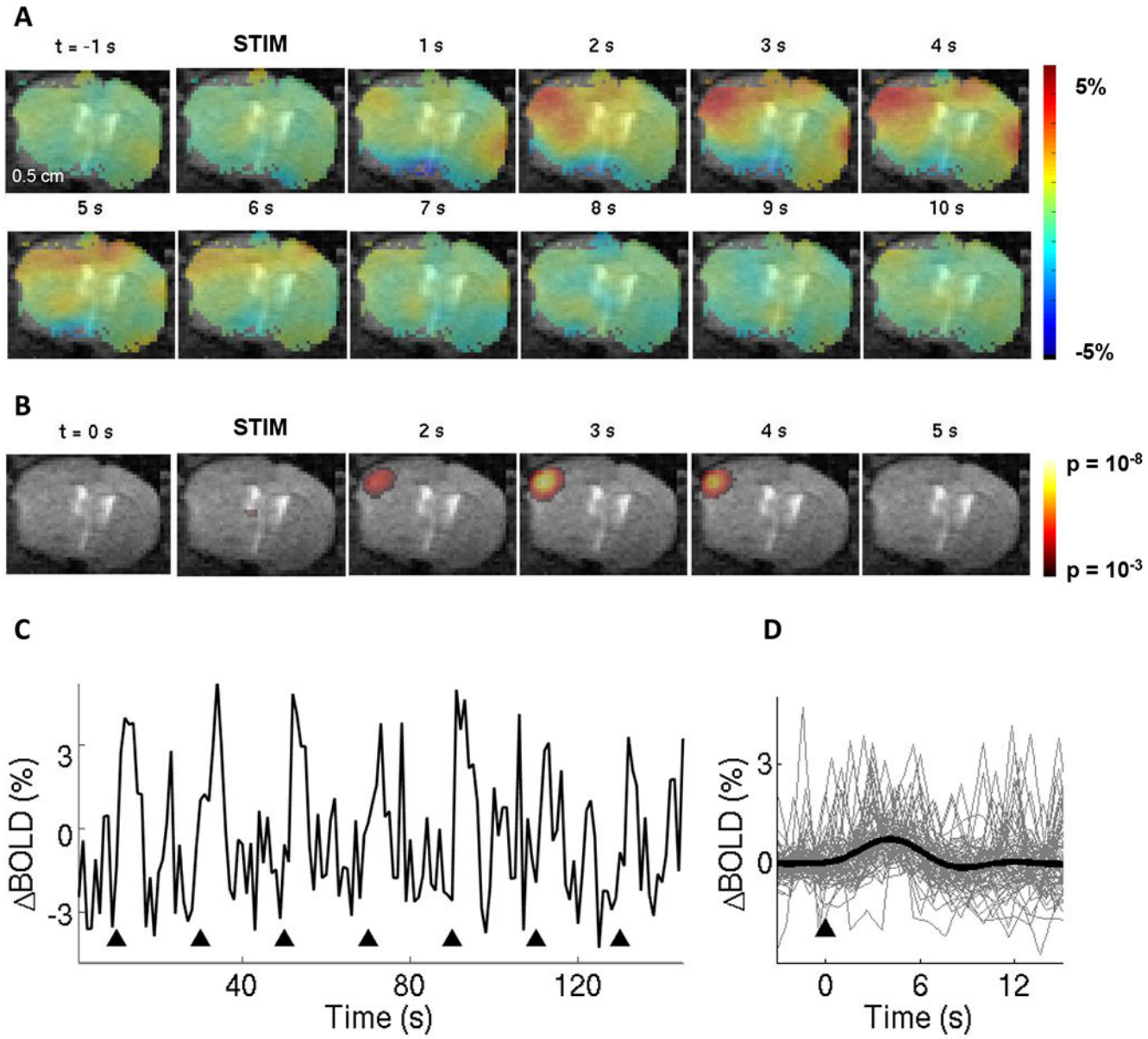

Figure 5. The BOLD signal under sedation with chlorprothixene

A. Spatiotemporal evolution of the BOLD signal change from a single slice cutting through the center of the evoked response, presented as ratio maps, in response to single 100-ms light pulses in a sedated Emx1-Cre/Ai32 subject.

B. Corresponding time-resolved p-maps. In this case, we made no assumptions about the shape of the HRF (i.e. using a “finite impulse response” model).

C. The BOLD signal time-course from the active ROI (defined by thresholding of the p-value map). Black arrowheads indicate onset on stimulation trials.

D. Superimposed BOLD response time-courses for 72 stimulus trials. The average is overlaid in thick black.